BIOCHEMISTRY
including biophysical chemistry & molecular biology

Article

pubs.acs.org/biochemistry

Different Hydration Patterns in the Pores of AmtB and RhCG Could Determine Their Transport Mechanisms

Sefer Baday,[†] Shihao Wang,[‡] Guillaume Lamoureux,*[,‡] and Simon Bernèche*[,†]

[†]Swiss Institute of Bioinformatics and Biozentrum University of Basel, Klingelbergstrasse 50/70, CH-4056 Basel, Switzerland

[‡]Department of Chemistry and Biochemistry and Centre for Research in Molecular Modeling (CERMM), Concordia University, 7141 Sherbrooke Street West, Montréal, Québec H4B 1R6, Canada

Supporting Information

ABSTRACT: The ammonium transporters of the Amt/Rh family facilitate the diffusion of ammonium across cellular membranes. Functional data suggest that Amt proteins, notably found in plants, transport the ammonium ion (NH_4^+), whereas human Rhesus (Rh) proteins transport ammonia (NH_3). Comparison between the X-ray structures of the prokaryotic AmtB, assumed to be representative of Amt proteins, and the human RhCG reveals important differences at the level of their pore. Despite these important functional and structural differences between Amt and Rh proteins, studies of the AmtB transporter have led to the suggestion that proteins of both subfamilies work according to the same mechanism and transport ammonia. We performed molecular dynamics simulations of the AmtB and RhCG proteins under different water and ammonia occupancy states of their pore. Free energy calculations suggest that the probability of finding NH_3 molecules in the pore of AmtB is negligible in comparison to finding water. The presence of water in the pore of AmtB could support the transport of proton. The pore lumen of RhCG is found to be more hydrophobic due to the presence of a phenylalanine conserved among Rh proteins. Simulations of RhCG also reveal that the signature histidine dyad is occasionally exposed to the extracellular bulk, which is never observed in AmtB. These different hydration patterns are consistent with the idea that Amt and Rh proteins are not functionally equivalent and that permeation takes place according to two distinct mechanisms.

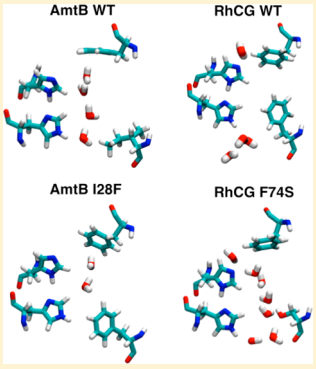

Proteins from the Amt/Rh family facilitate the transport of ammonium across cellular membranes. Functional studies have generally suggested that members of the Amt subfamily, notably found in plants, transport the ammonium ion (NH_4^+),[1−4] whereas the mammalian Rh proteins transport ammonia (NH_3).[5,6]

The elucidation of the structure of the prokaryotic AmtB transporter, the first from the Amt/Rh family, has brought essential new insights toward the understanding of the function of ammonium transporters.[7,8] Nevertheless, the mechanism of transport and the substrate of AmtB itself remain a matter of debate with important consequences because AmtB is often considered an archetype of the Amt subfamily. A close examination of the structural and functional data reveals many incompatible observations. On the basis of X-ray diffraction data, it was suggested that the pore of AmtB is occupied by ammonia molecules diffusing in single file.[7] Electronic density was, however, also observed in crystals grown in absence of ammonium salt, arguing against the above conclusion.[9] Although different functional studies based on transport assays, growth experiments, and pH measurements led to the suggestion that AmtB transports ammonia,[7,10] a critical assessment of these different approaches shows the difficulties in applying such measurements to AmtB and in interpreting the available data.[11] A mutational study has also highlighted the specific chemistry essential to transport in AmtB, supporting the idea of strong interactions with an ammonium ion rather than with neutral ammonia.[12] Incomplete or partial analyses of the available X-ray and functional data on AmtB have led to an amalgam between the function of Amt and Rh proteins, which are both often described as "ammonia channels".

Comparison of the X-ray structures of the AmtB[7] and RhCG[13] pores reveals significant differences (Figure 1). Although the two transporters share the same overall pore architecture, some residues at key positions differ.[14] First, the two phenylalanine residues forming a gate at the entrance of the pore lumen do not adopt the same conformation in the crystals of the two proteins. Whether this apparent difference is functionally important or not is unknown. Second, a threonine (Thr273) is found at the entrance of the pore lumen of AmtB, above the histidine dyad (His168/His318). Electronic density in that region of the pore was observed in RhCG crystals and attributed to a water molecule. Although both the threonine side chain and the water molecule present a hydroxyl group at similar positions, their mobilities are different and can potentially differentiate the two pores. Finally, in RhCG, a phenylalanine (Phe74) occupies a large portion of the pore at the level of the two signature histidine residues, whereas the pore of AmtB is unobstructed.

Received: January 4, 2013
Revised: September 6, 2013
Published: September 10, 2013

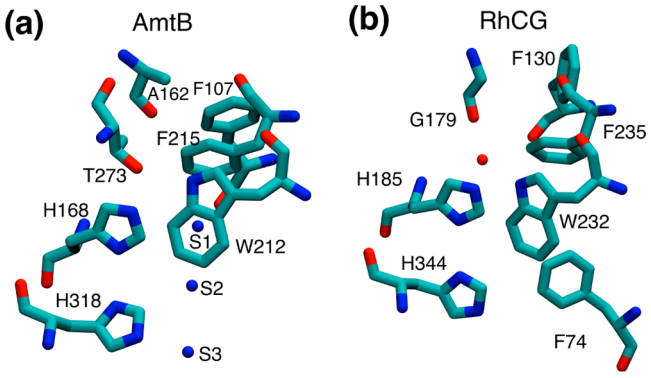

Figure 1. Details of the pores of the AmtB (a) and RhCG (b) proteins (PDB entries 1U7G and 3HD6). (a) Electronic density in the pore lumen of AmtB was attributed to three ammonia molecules putatively diffusing in single file. (b) In RhCG, electronic density just above His185 was attributed to a water molecule. In both schemes, the extracellular side is upward.

Among contentious elements is the possible presence of water molecules in the pore lumen of the ammonium transporters.[15] As we have shown in a previous study, water molecules in the pore can stabilize the charged NH_4^+ and conduct a proton, allowing for electrogenic transport in AmtB.[16] Water molecules could thus be determinant for the transport mechanism.

To better understand the similarities and differences between the Amt and Rh proteins, we perform molecular dynamics simulations of the AmtB and RhCG proteins. More specifically, we compare the ammonia and water occupancies in the pore of the two transporters. The simulations uncover important differences, notably at the level of the pore lumen, which is hydrophobic in RhCG but hydrophilic in AmtB. The RhCG simulations also reveal a pore exposing the histidine dyad to extracellular bulk water. Our study suggests that two distinct mechanisms sustain ammonium permeation in Amt and Rh proteins.

MATERIALS AND METHODS

Simulation Systems. The crystal structure from PDB entry 1U7G was used for the simulations of AmtB.[7] Residues Ser68, Pro126, and Leu255 were mutated to the corresponding amino acids in the wild-type (WT) sequence (F68, S126, and K255). Two protonation states for the histidine dyad His168/His318 were considered. In the first protonation state, hydrogen atoms are positioned on N^{δ} of His168 and Nε of His318. In the second protonation state, hydrogen atoms are on Nε of His168 and N^{δ} of His318. Membrane−protein systems were built using the CHARMM-GUI web service.[17] A membrane bilayer composed of 289 dimyristoylphosphatidylcholine (DMPC) lipids was assembled around the trimeric AmtB structure and solvated with more than 20 000 TIP3P water molecules. Ions (55 K^+ and 61 Cl^-) were added to reproduce a 0.15 M KCl concentration and to obtain a neutral system. The tetragonal unit cell of 114 × 114 × 90 Å^3 contains about 120 000 atoms.

The RhCG system was built following the same procedure, using PDB entry 3HD6. The structure of two missing loops (residues 35−52 and 362−383) was modeled using cyclic coordinate descent (CCD) loop modeling method[18] implemented in the Rosetta program.[9] The histidine dyad in the pore is neutral with hydrogen atoms positioned on N^{δ} of His185 and Nε of His344. (By analogy with AmtB, this protonation state is assumed to be the functional form of the pore.) The RhCG trimer is surrounded by a membrane bilayer of 321 DMPC lipids, solvated by 21 407 TIP3P water molecules and 0.15 M KCl. The system containing 121 237 atoms holds in an orthogonal box of 115 × 122 × 83 Å^3. The systems for the AmtB and RhCG mutants were constructed by changing the side-chain atoms of the targeted amino acid in the equilibrated wild-type systems.

All systems were equilibrated using CHARMM (version c34b2)[19] and simulated for 100 ns using the NAMD simulation package (version 2.7b4) [20] with the CHARMM 27 force field.[21] Particle-mesh Ewald method [22] was applied for the calculation of electrostatic interactions with a grid spacing of 1 Å. The cutoff distance for van der Waals interactions was taken at 12 Å with a switching function starting at 10 Å. Time step for the integration of the motion was set to 1 fs. Short-range nonbonded interactions were calculated every 2 steps and long-range interactions every 4 steps. Simulations were performed in an isothermal−isobaric ensemble with a pressure of 1 atm and a temperature of 315 K. Parameters for ammonia (NH_3) were taken from the optimized potentials for liquid simulations (OPLS) model.[23] According to this model, the free energy of solvation of NH_3 in TIP3P water molecules is 2.7 kcal/mol higher than that of H_2O, comparable to the experimental free energy difference of 2.0 kcal/mol.[24] If the small difference has an impact on the simulations, it would bias our results toward a higher occupancy probability of NH_3 in the hydrophobic pore of the transporters.

Free-Energy Perturbation Calculations. Free-energy perturbation (FEP) simulations [25] were used to calculate the free energy difference between water and ammonia for different occupancy states of the AmtB pore. For these FEP calculations performed with NAMD, the molecular system contains a hybrid residue representing simultaneously both an ammonia and a water molecule. Interactions of the atoms of this residue with surrounding atoms are scaled by a thermodynamic parameter λ. When $\lambda = 0$, only the interactions of the water molecule with surrounding atoms are considered, whereas only the interactions of ammonia molecule are considered when $\lambda = 1$. A linear combination of these interaction energies is applied when λ is between 0 and 1. There is no interaction between the ammonia and water molecules, except that their heavy atoms are linked by a harmonic tether with a force constant of 500 kcal/(mol·Å^2).[26]

The reaction coordinate (λ) in the FEP simulations is discretized into windows of width 0.1 for λ ranging from 0.1 to 0.9 and these windows were simulated for 200 ps (first 20 ps for equilibration). At the end points, λ was progressively increased with windows at 0, 0.001, 0.01, 0.05, and 0.95, 0.99, 0.999, 1 that were simulated for 100 ps (first 10 ps for equilibration). For each perturbation calculation, the combined forward and backward simulations amounted to a total simulation time of 4.8 ns. Free energy differences and statistical errors were calculated by combining the forward and backward configurational ensembles using the Bennett acceptance ratio (BAR) method as implemented in the ParseFEP toolkit[27] of the VMD visualization platform.[28]

FEP simulations were performed with a monomeric AmtB system, containing 185 DMPC, 33 K^+, and 35 Cl^-, for a total of about 67 000 atoms (box size 92 × 78 × 92 Å^3). In the FEP simulations, the hybrid residue and water molecules were restrained along the z-coordinate (normal to the membrane) to maintain them in a single file. For each site, a harmonic flat-bottom restraint defined in function of the distance to the center of mass of the Cα of His168 and His318 was applied. Figure S1 of the Supporting Information illustrates the boundaries beyond

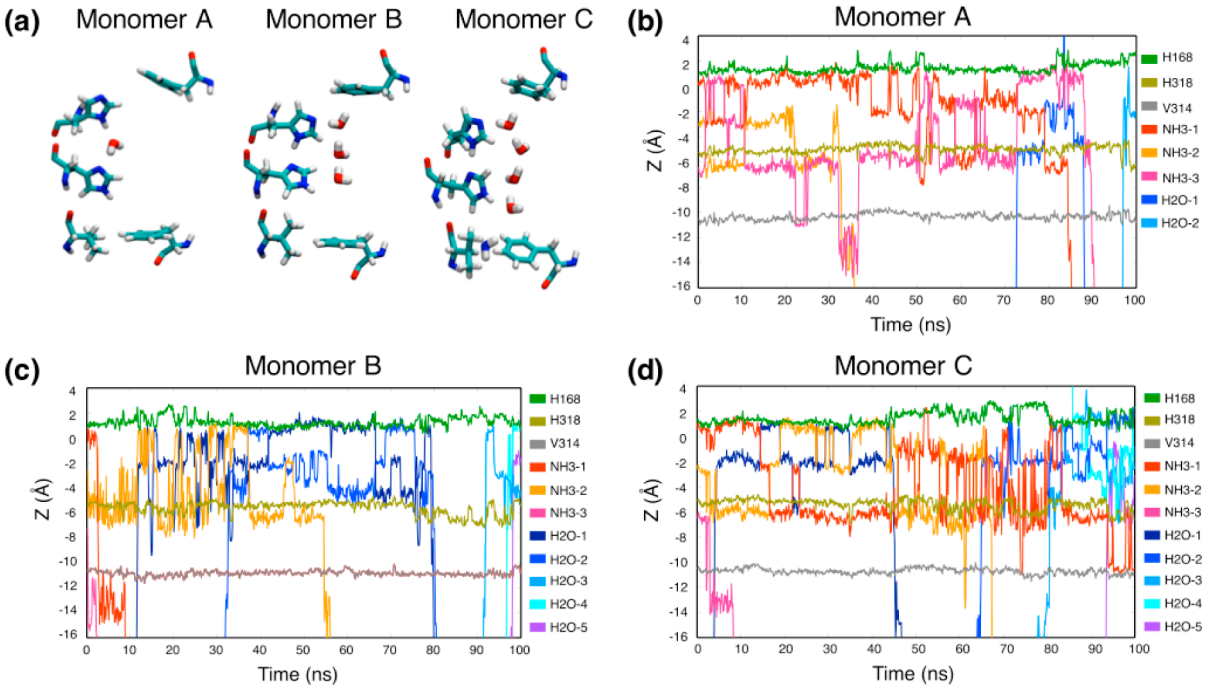

Figure 2. Simulation of AmtB initiated with three ammonia molecules in each pore. (a) Configurations at the end of the simulation showing key residues and water molecules in the pore for all three monomers. (b)−(d) Positions along *Z*-axis of ammonia and water molecules in the pore of monomers A, B, and C. $Z = 0$ corresponds to the center of mass of the protein. Some water molecules entering the pore only briefly are not shown in the time series.

which the restraint is effective for each site. The perturbation calculations in bulk water were performed on a system containing 284 water molecules with dimensions of $20 \times 20 \times 20$ Å^3 at a constant pressure of 1 atm.

RESULTS

Stability of Ammonia Molecules in the Pore of AmtB. To first investigate the stability of ammonia molecules in the pore of AmtB, we performed a simulation of the AmtB trimer starting with three ammonia molecules placed in each pore at positions corresponding to experimental electron density maxima. In all monomers, all three ammonia molecules leave the pore (some after only a few nanoseconds of simulation, others after 80 or 90 ns). At the end of the simulation, the pores of two of the three monomers are filled with three or four water molecules (Figure 2a). In monomer A, in the last few nanoseconds of the 100 ns simulation, a water molecule inserts between the two histidines residues. A similar conformation is more extensively sampled in another simulation (see Figure 3c below). Overall, the trajectories presented in Figure 2 show that ammonia molecules are metastable in the AmtB pore and are replaced by water molecules on the time scale of the simulation.

Stability of Water Molecules in the Pore of AmtB. To confirm water stability in the AmtB pore, two additional simulations of the trimeric system were performed, with and without water molecules initially present in the pore. Water molecules that were placed beforehand in the pore undergo many exchanges with water molecules from the cytosolic vestibule (see Figure S2 of the Supporting Information). In simulations in which the pore was initially empty, water molecules are seen entering the pores and occupying up to four distinct binding sites. Figure 3a shows conformations of water molecules inside the pore at the end of a simulation of the AmtB trimer initiated with three empty pores. The time series of Figure 3b,c show that water molecules filled up the pore in less than 10 ns in monomers A and B. In monomer C, three water molecules fill up the pore after about 35 ns. In this situation, water molecules usually form a stable chain as illustrated in Figure 3a. Water molecules exchange positions many times over the whole simulation, with entry and exit of some of them. All movement of water molecules in and out of the pore happen from the intracellular side, except one event (see Figure 3d, at $t \approx 55$ ns). This shows that the gate formed by the Phe residues on the extracellular side of the pore has extremely low permeability to water, in agreement with experiments showing that AmtB does not conduct water.[7] In monomer B, a water molecule intercalates between the two histidine residues in the interval $t = 30-40$ ns, and again starting at $t = 60$ ns (see Figure 3c). The water molecule is metastable in this position and is replaced a few times over the remaining 40 ns. When a water molecule is found between residues His168 and His318, the two side chains are farther away from each other, and His168 Nε is no longer in position to stabilize water molecules in the pore. Once the intercalated water molecule leaves, the two histidine side chains regain their initial conformation. Figure 4 presents the density profile describing the average water occupancy in AmtB extracted from the simulation initiated with empty pores. The density profile for each monomer is shown in Figure S3 of the Supporting Information.

We also performed simulations of the AmtB trimer considering an alternative protonation state of the histidine dyad with hydrogen atoms on Nε of His168 and N$^{\delta}$ of His318, without water molecules initially bound to the pore. The density profile (reported in Figure 4) shows that water molecules are less stable for this reverse protonation state than for the canonical state, in agreement with our previous work.[15] Nevertheless, a water chain of three or more water molecules is observed for a non-negligible fraction of the simulation time for the reversed protonation state, which would allow proton diffusion as recently proposed.[16] The standard deviation of the density profiles,

dx.doi.org/10.1021/bi400015f | *Biochemistry* 2013, 52, 7091−7098

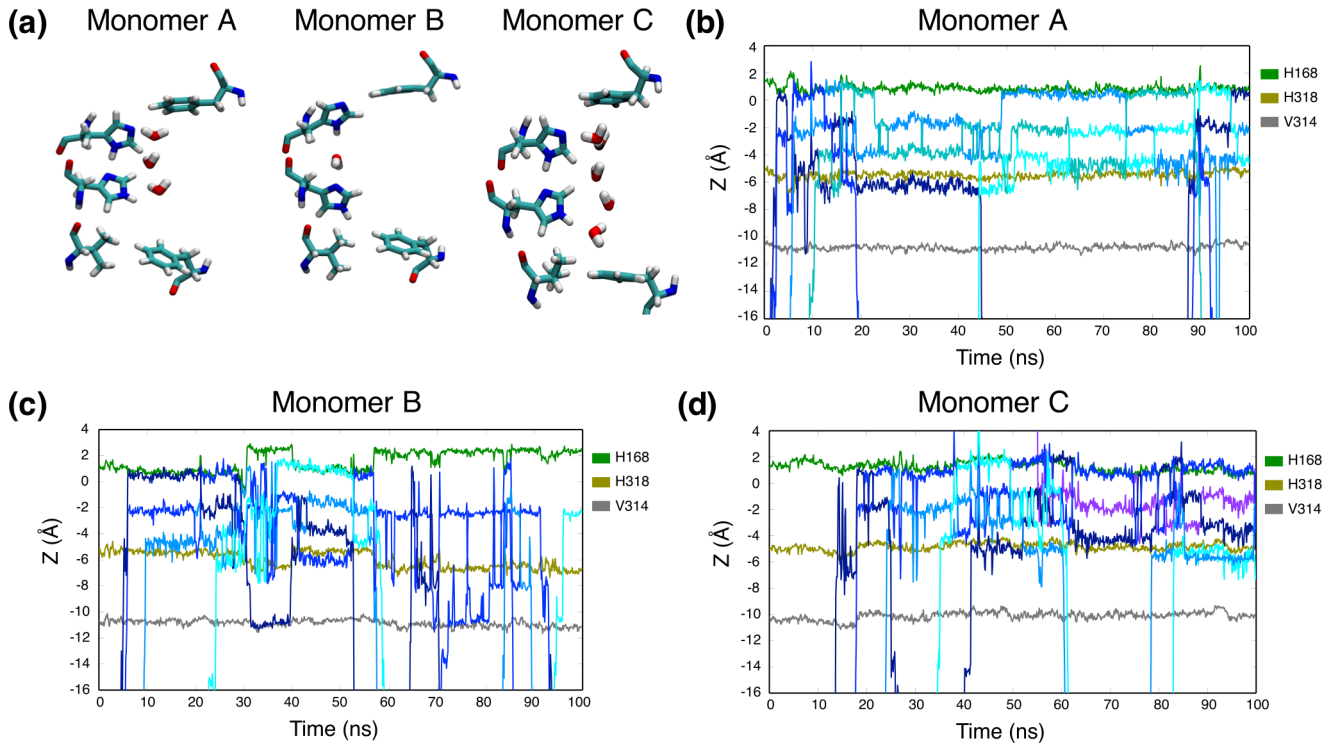

Figure 3. Simulation of AmtB started with empty pores. (a) Configurations of water molecules in the pores of all monomers at the end of the simulation. (b)−(d) Positions along the *Z*-axis of water molecules in the pore of monomers A, B, and C. Traces that are not labeled in the legend correspond to water molecules. $Z = 0$ corresponds to the center of mass of the protein.

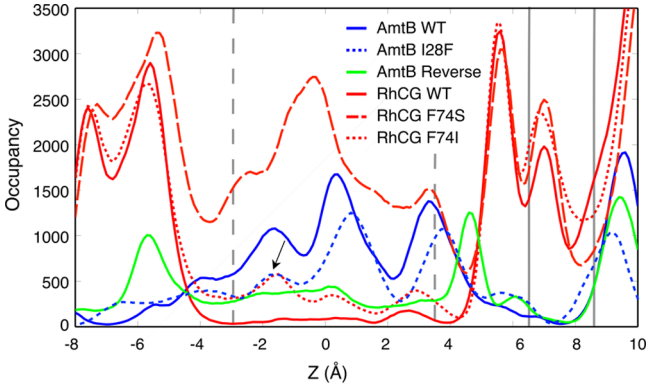

Figure 4. Water occupancy in pore of different constructs of AmtB and RhCG. In all cases, histograms were calculated from 100 ns simulations initiated with empty pores and averaged over the three monomers. The *Z* position was calculated relative to the center of mass of the Cα of the two histidines residues lining the pore. The gray dashed lines indicate the position of the Nε atoms of these two histidines. The solid lines correspond to the position of the Cα of the two phenylalanines on the extracellular side of the pore. The meaning of the arrow is described in the text.

calculated by dividing the simulations in five intervals, is shown in Figure S4 of the Supporting Information.

Relative Stabilities of Water and Ammonia in the Pore of AmtB. The simulations presented above suggest that NH_3 and H_2O molecules may both occupy the pore of AmtB. To have a more precise idea of their relative stability, we have performed FEP calculations in which a water molecule is alchemically transformed into an ammonia molecule both in water bulk and in the pore of AmtB. The free energy difference between transferring an ammonia (A) or a water (W) molecule from the bulk to the pore can be expressed as

$$\begin{aligned}\Delta\Delta G &= [G(A_{pore}) - G(A_{bulk})] - [G(W_{pore}) - G(W_{bulk})] \\ &= [G(A_{pore}) - G(W_{pore})] - [G(A_{bulk}) - G(W_{bulk})] \\ &= \Delta G(W_{pore}\rightarrow A_{pore}) - \Delta G(W_{bulk}\rightarrow A_{bulk}) \end{aligned} \quad (1)$$

The perturbation calculation in the bulk water system in which a water molecule is alchemically transformed to ammonia (second term of eq 1) yields a free energy difference of +2.7 ± 0.1 kcal/mol (BAR estimate), comparable to the difference of experimental solvation free energy for water and ammonia of +2 kcal/mol.[24] Several similar FEP calculations were performed in the pore (first term of eq 1) with various occupancy states. For these calculations, water and ammonia molecules in the pore were restrained to their respective binding sites (see Materials and Methods). Results from these calculations are reported in Table 1. The free energy differences for transforming a water molecule into ammonia in the pore are between 0.9 and 4.0 kcal/mol. The average of the different perturbation calculations is +2.8 kcal/mol, which yields an average free energy difference between the transfer of water and ammonia from bulk water to the pore, $\Delta\Delta G$, of about +0.1 kcal/mol. Given the uncertainty of the calculations it implies that, on average, the transfer of a water molecule from bulk water into the pore is energetically equivalent to the transfer of an ammonia molecule. These results are comparable to those of Luzhkov et al.,[29] who calculated a $\Delta\Delta G$ of +2.0 kcal/mol for the transformation aaa → waa, whereas we report +1.0 kcal/mol (Table 1). Accordingly, potential of mean force calculations by Lin et al. have shown little difference between the energetics of ammonia and water in

dx.doi.org/10.1021/bi400015f | *Biochemistry* 2013, 52, 7091−7098

Table 1. Free Energy of Various Perturbations in the Pore of AmtB (in kcal/mol)

perturbation[a]	forward	backward	average	BAR estimate	$\Delta\Delta G$
www → aww	1.7	−1.6	1.6	0.9 ± 0.1	−1.8 ± 0.2
aww → aaw	3.2	−4.1	3.6	2.5 ± 0.2	−0.3 ± 0.3
aaw → aaa	3.4	−3.5	3.4	3.7 ± 0.1	1.0 ± 0.2
www → wwa	3.9	−4.7	4.3	3.5 ± 0.1	0.7 ± 0.2
wwa → waa	4.6	−3.6	4.1	4.0 ± 0.1	1.3 ± 0.2
waa → aaa	2.4	−0.9	1.6	1.7 ± 0.2	−1.0 ± 0.3
www → waw	3.6	−3.2	3.4	3.6 ± 0.2	0.9 ± 0.3
awa → aaa	3.7	−3.8	3.7	2.9 ± 0.1	0.2 ± 0.2

[a]Triplets denote the occupancy state of sites S1, S2, and S3 as identified in Figure S1 of the Supporting Information (w = H_2O, a = NH_3). $\Delta\Delta G$ = (BAR estimate) − 2.7 ± 0.1 kcal/mol, as defined in the text.

the pore of AmtB.[30] Ullmann et al. also found comparable binding free energies for ammonia and water in sites S1−S4 of Amt-1 from *Archaeoglobus fulgidus* through the use of Monte Carlo simulations.[31]

However, the binding free energy difference is not the only factor determining the probability of observing either water or ammonia molecules in the pore of AmtB. The concentration of both molecules in the environment of the transporter needs to be taken into account as well. We can incorporate the effect of concentration using the following Boltzmann relation:

$$\frac{P_{NH_3}}{P_{H_2O}} = \frac{[NH_3]}{[H_2O]} e^{-\Delta\Delta G/k_B T} \quad (2)$$

where P_{NH_3}/P_{H_2O} is the relative binding probability of ammonia versus water in the pore of AmtB, $[NH_3]/[H_2O]$ is the ratio of ammonia and water concentrations in solution, $\Delta\Delta G$ is the binding free energy difference between water and ammonia, k_B is the Boltzmann constant, and T is the temperature.

For a hypothetical concentration of 1 mM for NH_3, which is high considering that the AmtB transporter is reportedly expressed at NH_4^+ concentrations of 50 μM or less,[32] we get a relative probability of $P_{NH_3}/P_{H_2O} = 1.5 \times 10^{-5}$, with $[H_2O] = 55$ M, $\Delta\Delta G = 0.1$ kcal/mol, and $k_B T$ (315 K) = 0.626 kcal/mol. With $\Delta\Delta G = -1.9$ kcal/mol corresponding to the most favorable transfer of ammonia to the pore of AmtB (first line of Table 1), the relative probability is $P_{NH_3}/P_{H_2O} = 3.8 \times 10^{-4}$.

Thus, even in artificially high ammonia concentration corresponding to 10 times the one expected in the crystallization experiments of Khademi et al.,[7] the probability of finding an ammonia molecule in the pore of AmtB is less than a thousandth of that of a water molecule. The probability of finding three ammonia molecules in the pore would be a factor 10^{-10} lower than that of finding three water molecules. Taken together, the simulations and free energy calculations suggest that the pore of the AmtB transporter in its resting state is occupied by water molecules for a non-negligible fraction of the time, and that the presence of NH_3 is highly unlikely.

Stability of Ammonia and Water Molecules in the Pore of RhCG. To assess the stability of ammonia molecules in the pore of the RhCG protein, we performed a simulation starting with three ammonia molecules bound to the pore. Figure 5a displays the final conformation of molecules in the pore of the three monomers. The time series in Figure 5b,d shows that the three ammonia molecules leave the pore in all three monomers. In monomer A, an ammonia molecule stays in the vicinity of the pore, just below His344. Contrary to what was observed for AmtB, the pores remain mostly empty. In monomer A, transient visits of NH_3 and H_2O are seen, with a higher frequency in the first half of the simulation. In monomer C, the two histidines lining the pore (His185/His344) rotate and expose a polar nitrogen to the pore lumen, attracting water molecules (see Figure 5d). The stabilization of water molecules in the pore favors the reorientation of the Phe74 side chain. In AmtB, the rotation of the histidine dyad was considered as a potential mechanism allowing for proton transport in the pore, but free energy calculations suggest that it is energetically prohibitive.[16] Whether such conformational change could play a role in the transport of ammonium in RhCG remains to be seen and will require further calculations.

We also carried out a simulation of RhCG starting with empty pores. Analysis of the trajectory shows that although water molecules can occasionally enter the pore, they cannot find stable positions and even less form a chain of three or more molecules. No rotation of the two histidines and water stabilization were observed in this second simulation. The density profile presented in Figure 4 illustrates that only a small number of water molecules are found in the pore at the level of the histidine dyad. Figure 6a shows the final conformation of the pore and water molecules in its vicinity for each monomer. A simulation initiated with water molecules in the pores yielded similar results (see Figure S4b of the Supporting Information). Interestingly, in all monomers, a water molecule is seen forming a hydrogen bond with His185 and the carbonyl group of Gly179, occupying a position also identified by X-ray crystallography (see Figure 1b). The simulations further reveal that a chain of water molecules can transiently form between His185 and the extracellular bulk (Figure 6b,c), which opens a direct access to His185. Such conformation is not observed in AmtB, in which access to His168 is blocked by two stacked phenylalanine residues. A comparison of the X-ray structures of RhCG and AmtB reveals subtle but important differences between the two proteins in that region of the pore. First, in the conformations captured by X-ray crystallography, the aromatic rings of the two phenylalanine residues at the entrance of the pore are parallel in AmtB but perpendicular in RhCG (see Figure 1). These conformations remain predominant during the MD simulations for AmtB and RhCG (Figures S5 and S6 of the Supporting Information). Second, in AmtB, Thr273 makes a hydrogen bond with Trp212 and occasionally with His168 during simulations, whereas in RhCG a water molecule is found at that position that interacts with both His185 and Trp232. Simulations show that this water molecule can also form a hydrogen bond with water molecules at the level of the two phenylalanine residues (Phe130/Phe235).

Simulation of AmtB and RhCG Mutants. The simulations reported above suggest that residue Phe74 prevents the formation of a stable water chain in the pore of RhCG. Sequence

dx.doi.org/10.1021/bi400015f | *Biochemistry* 2013, 52, 7091−7098

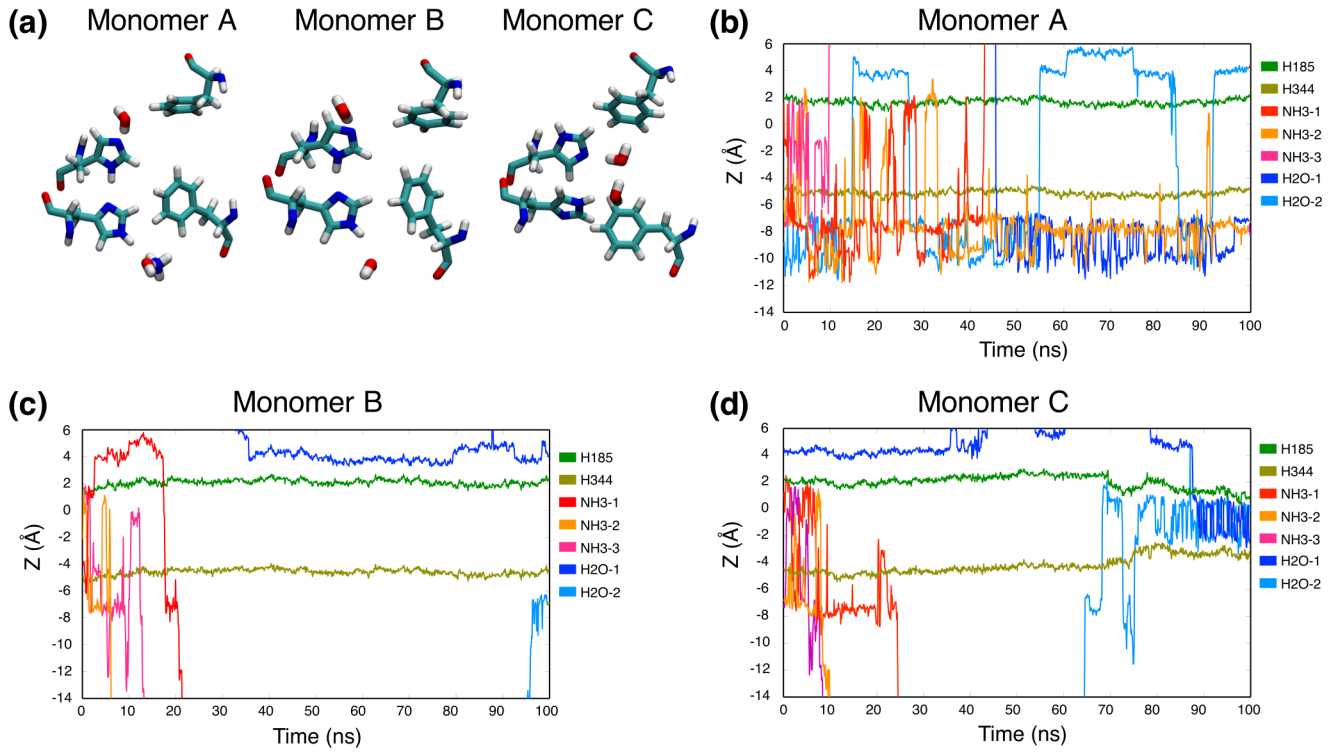

Figure 5. Simulation of RhCG performed with three ammonia molecules initially bound to each pore. (a) Configuration of the pore at the end of the simulation for all three monomers. (b)−(d) Positions along the *Z*-axis of ammonia and water molecules in the pore of monomers A, B and C. $Z = 0$ corresponds to the center of mass of the protein. A few ammonia and water molecules are seen going back and forth in monomer A. No such transition in seen in monomer B. In monomer C, a configuration is observed in which F74 is tilted down, which allows two water molecules to occupy the pore.

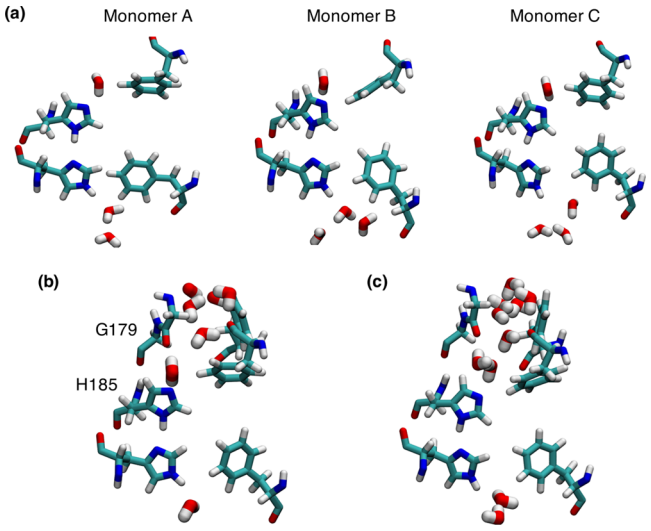

Figure 6. Simulation of RhCG started with empty pores. (a) Final configuration of the molecules in the pore for each monomer after 100 ns of simulation. All three pores remained empty, while a water molecule was seen above His185 at the position of a crystallographic water (see Figure 1). (b), (c) Water molecules observed in greater number in upper part of pore, forming a discontinuous (b) or continuous (c) chain. The presence of these water molecules suggests that an NH_4^+ molecule from the extracellular bulk could reach His185.

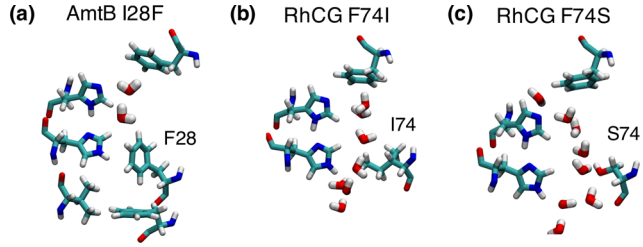

Figure 7. Representative configurations from the AmtB I28F, RhCG F74I, and RhCG F74S mutant simulations. (a) In the pore of the I28F mutant of AmtB, a constriction at the level of His318 and Phe28 prevents the formation of a water wire. Water molecules are, however, frequently seen in the upper part of the pore. (b) Reciprocally, in RhCG, replacing Phe74 by an isoleucine residue allows the formation of a water wire spanning the whole pore lumen. This configuration is often observed but not as frequently as in AmtB WT. (c) Such a water chain is more frequently observed in the pore of RhCG F74S, where water molecules are even more stable and numerous than in AmtB WT.

and structure alignments indicate that residue Phe74 in RhCG corresponds to residue Ile28 in AmtB.[14] We hypothesized that amino acids at these positions are determinant for the formation or absence of a water chain in the pore lumen and that mutating the amino acids could confer the properties of one transporter to the other. We thus simulated both the I28F mutant of AmtB and F74I mutant of RhCG with the pore lumens initially empty. For most of the AmtB I28F mutant simulation, two water molecules are present in the pore (Figure 7a). As illustrated by the density profile in Figure 4, the presence of the phenylalanine does not on its own prevent water molecules from occupying the pore, but it significantly decreases the water density in its lower part (arrow on Figure 4) and by the same occasion the probability of observing a continuous chain of water. The hydration of the upper part of the pore seems to be favored by the polar Nε atom of His168, which faces the pore lumen and helps stabilizing a water molecule. On the other hand, a continuous water chain is

dx.doi.org/10.1021/bi400015f | *Biochemistry* 2013, 52, 7091−7098

observed for most of the simulation time in one monomer of the RhCG F74I mutant (Figure 7b). However, the lack of a polar group facing the pore, such as His168 Nε in AmtB, seems to limit the overall hydration of the pore (Figure 4).

Interestingly, in the related RhAG protein, mutation of the equivalent phenylalanine residue to a serine (F65S) is associated with overhydrated hereditary stomatocytosis (OHSt) of red cells, which is a hemolytic anemia characterized by monovalent cation leaks.[33,34] We have performed a 100-ns long simulation of the RhCG F74S mutant. In all three monomers, water molecules occupy the pore in a large enough amount to potentially accommodate a cation (Figure 7c). The pore of the RhCG F74S mutant is more hydrophilic than that of wild-type AmtB (Figure 4) and stabilizes water molecules through a distinct hydrogen-bonding scaffold (see also Figure S7 of the Supporting Information). In conclusion, the presence of a phenylalanine in the pore of RhCG at the level of the histidine dyad has a direct impact on the hydration of the pore. Moreover, the histidine residues on the extracellular side (His168 in AmtB and His185 in RhCG) do not have the same environment and favor different hydration patterns of the pore. In RhCG, His185 contributes to the stabilization of water molecules at the level of the two external phenylalanine residues and not at the level of the two signature histidines; it is the opposite for His168 in AmtB.

DISCUSSION

To better understand the transport mechanism in the related but functionally different AmtB and RhCG transporters, we have performed simulations under different occupancy states of the pore of both proteins. The simulations and free energy calculations show that, contrary to what is often assumed, the pore of the AmtB protein is more likely to be occupied by water molecules than by ammonia. Because the concentration of water is much larger than that of ammonia, the probability of finding a water molecule at any binding site of the pore is at least 2.6×10^3 times that of an ammonia molecule according to our estimates (using the binding energy differences from Table 1 and assuming an NH_3 concentration of 1 mM). The low binding affinity of the pore for ammonia molecules, comparable to that for water molecules, combined with the low concentration of ammonia implies that the permeation in AmtB cannot be described as a single file diffusion of ammonia, as was proposed on the basis of X-ray diffraction data.[7] The presence of electronic density in the pore of AmtB observed in crystals grown without ammonium salt supports the idea that the pore lumen can be occupied by water molecules.[8,15] As was shown previously, these water molecules contribute to the stabilization of NH_4^+ in site S2, from where it can spontaneously transfer a proton to His168 and diffuse as NH_3.[16] The present work confirms that a chain of water can transiently form in the pore of AmtB when the histidine dyad is in its reverse protonation state. Such a chain could serve as a proton wire from His168 to His318, allowing for the reset of the histidine dyad protonation state in an electrogenic transport involving the cotransport of NH_3 and H^+.[16]

Our simulations of RhCG have shown that NH_3 can diffuse freely in and out of the pore, in agreement with free energy calculations performed on Rh50, another Rhesus transporter of known structure.[35] In contrast with AmtB, the water occupancy in the pore is much less in RhCG. The presence of a phenylalanine, strongly conserved in the Rh protein family, occupies a large portion of the pore at the level of the histidine dyad and prevents the formation of a stable water chain. This residue is, however, not the only determinant of the pore hydration. The fact that the polar nitrogen of His185 is pointing toward the extracellular bulk rather than toward the pore lumen, like His168 in AmtB, seems to also contribute to the reduction of the hydrophilicity of the pore. If His185 has access to water molecules coming from the extracellular bulk, it is less likely to be available for interaction with water in the hydrophobic pore. Thus, the electrogenic transport mechanism proposed for AmtB may not apply to RhCG, in line with the generally accepted idea that Rh proteins sustain an electroneutral transport of ammonia. Interestingly, the RhCG mutant F74S (and to a lesser extent F74I) leads to a higher hydration of the pore and the formation of a water chain at the level of the histidine dyad similar to the one observed in AmtB. We surmise that these mutants could potentially sustain electrogenic transport, though we have not attempted here a full description of the energetics underlying the permeation mechanism. The increased hydration of the pore as observed in the simulation of RhCG F74S can potentially explain the permeation of monovalent cations reported for the homologous RhAG F65S mutant, which is characteristic of overhydrated stomatocytic red blood cells.[33,34]

The transport mechanism in wild-type RhCG remains unresolved, but our simulations suggest some elements of answer. Contrary to what is observed in AmtB, the upper part of the RhCG pore, at the level of Phe130 and Phe235, is partially hydrated, allowing a continuous chain of water molecules to form between His185 and the extracellular water bulk (Figure 6c). His185 seems to be optimally placed to accept a proton from an incoming NH_4^+, which could further diffuse down the pore as NH_3. Further investigation will be required to elucidate the complete permeation mechanism in RhCG. Nevertheless, our simulations and free energy calculations suggest that small variations in the sequence of ammonium transport proteins, notably at the level of their pore lumen, might have important functional consequences.

ASSOCIATED CONTENT

Supporting Information

Boundaries along the *Z*-axis of the flat-bottom restraints applied to water and ammonia molecules during the free energy perturbation calculations, residence time for water molecules in the pore of AmtB WT, water occupancy in the pore of each monomer of AmtB WT and RhCG WT, water occupancy in the pore of the different constructs of AmtB and RhCG with standard deviation, relative orientation of the aromatic groups of two phenylalanine residues in AmtB and RhCG, rotameric states of key aromatics residues around the pore of AmtB WT and RhCG WT, and structural order of the water molecules in the pore of AmtB WT and RhCG F74S. This material is available free of charge via the Internet at http://pubs.acs.org.

AUTHOR INFORMATION

Corresponding Authors

*G. Lamoureux. Tel.: (+1) 514-848-2424 ext 5314. E-mail: guillaume.lamoureux@concordia.ca.

*S. Bernèche. Tel.: +41 61 267 2003. E-mail: simon.berneche@unibas.ch.

Funding

This work was supported by a grant from the Swiss National Science Foundation to S. Bernèche (SNF Professorship No. 139205) and by an FQRNT Nouveaux chercheurs grant to G.L. Computational resources were provided through a grant from the Swiss National Supercomputing Centre (CSCS) under

project ID s241, by the Basel Computational Biology Center, and through an allocation from Calcul Québec.

Notes

The authors declare no competing financial interest.

REFERENCES

(1) Ninnemann, O., Jauniaux, J. C., and Frommer, W. B. (1994) Identification of a high affinity NH4+ transporter from plants. *EMBO J. 13*, 3464−3471.

(2) Siewe, R. M., Weil, B., Burkovski, A., Eikmanns, B. J., Eikmanns, M., and Krämer, R. (1996) Functional and genetic characterization of the (methyl)ammonium uptake carrier of Corynebacterium glutamicum. *J. Biol. Chem. 271*, 5398−5403.

(3) Marini, A. M., Soussi-Boudekou, S., Vissers, S., and Andre, B. (1997) A family of ammonium transporters in Saccharomyces cerevisiae. *Mol. Cell. Biol. 17*, 4282−4293.

(4) Ludewig, U., von Wirén, N., and Frommer, W. B. (2002) Uniport of NH4+ by the root hair plasma membrane ammonium transporter LeAMT1;1. *J. Biol. Chem. 277*, 13548−13555.

(5) Ripoche, P., Bertrand, O., Gane, P., Birkenmeier, C., Colin, Y., and Cartron, J. P. (2004) Human Rhesus-associated glycoprotein mediates facilitated transport of NH_3 into red blood cells. *Proc. Natl. Acad. Sci. U. S. A. 101*, 17222−17227.

(6) Mouro-Chanteloup, I., Cochet, S., Chami, M., Genetet, S., Zidi-Yahiaoui, N., Engel, A., Colin, Y., Bertrand, O., and Ripoche, P. (2010) Functional reconstitution into liposomes of purified human RhCG ammonia channel. *PLoS One 5*, e8921.

(7) Khademi, S., O'Connell, J., Remis, J., Robles-Colmenares, Y., Miercke, L. J., and Stroud, R. M. (2004) Mechanism of ammonia transport by Amt/MEP/Rh: structure of AmtB at 1.35 Å. *Science 305*, 1587−1594.

(8) Zheng, L., Kostrewa, D., Bernèche, S., Winkler, F. K., and Li, X. D. (2004) The mechanism of ammonia transport based on the crystal structure of AmtB of Escherichia coli. *Proc. Natl. Acad. Sci. U. S. A. 101*, 17090−17095.

(9) Wang, C., Bradley, P., and Baker, D. (2007) Protein−protein docking with backbone flexibility. *J. Mol. Biol. 373*, 503−519.

(10) Soupene, E., He, L., Yan, D., and Kustu, S. (1998) Ammonia acquisition in enteric bacteria: physiological role of the ammonium/methylammonium transport B (AmtB) protein. *Proc. Natl. Acad. Sci. U. S. A. 95*, 7030−7034.

(11) Javelle, A., Lupo, D., Li, X. D., Merrick, M., Chami, M., Ripoche, P., and Winkler, F. K. (2007) Structural and mechanistic aspects of Amt/Rh proteins. *J. Struct. Biol. 158*, 472−481.

(12) Fong, R. N., Kim, K. S., Yoshihara, C., Inwood, W. B., and Kustu, S. (2007) The W148L substitution in the Escherichia coli ammonium channel AmtB increases flux and indicates that the substrate is an ion. *Proc. Natl. Acad. Sci. U. S. A. 104*, 18706−18711.

(13) Gruswitz, F., Chaudhary, S., Ho, J. D., Schlessinger, A., Pezeshki, B., Ho, C. M., Sali, A., Westhoff, C. M., and Stroud, R. M. (2010) Function of human Rh based on structure of RhCG at 2.1 Å. *Proc. Natl. Acad. Sci. U. S. A. 107*, 9638−9643.

(14) Zidi-Yahiaoui, N., Callebaut, I., Genetet, S., Le Van Kim, C., Cartron, J. P., Colin, Y., Ripoche, P., and Mouro-Chanteloup, I. (2009) Functional analysis of human RhCG: comparison with E. coli ammonium transporter reveals similarities in the pore and differences in the vestibule. *Am. J. Physiol.: Cell Physiol. 297*, C537−C547.

(15) Lamoureux, G., Klein, M. L., and Bernèche, S. (2007) A stable water chain in the hydrophobic pore of the AmtB ammonium transporter. *Biophys. J. 92*, L82−L84.

(16) Wang, S., Orabi, E. A., Baday, S., Bernèche, S., and Lamoureux, G. (2012) Ammonium transporters achieve charge transfer by fragmenting their substrate. *J. Am. Chem. Soc. 134*, 10419−10427.

(17) Jo, S., Kim, T., Iyer, V. G., and Im, W. (2008) CHARMM-GUI: a web-based graphical user interface for CHARMM. *J. Comput. Chem. 29*, 1859−1865.

(18) Canutescu, A. A., and Dunbrack, R. L. (2003) Cyclic coordinate descent: A robotics algorithm for protein loop closure. *Protein Sci. 12*, 963−972.

(19) Brooks, B. R., Brooks, C. L., Mackerell, A. D., Nilsson, L., Petrella, R. J., Roux, B., Won, Y., Archontis, G., Bartels, C., Boresch, S., Caflisch, A., Caves, L., Cui, Q., Dinner, A. R., Feig, M., Fischer, S., Gao, J., Hodoscek, M., Im, W., Kuczera, K., Lazaridis, T., Ma, J., Ovchinnikov, V., Paci, E., Pastor, R. W., Post, C. B., Pu, J. Z., Schaefer, M., Tidor, B., Venable, R. M., Woodcock, H. L., Wu, X., Yang, W., York, D. M., and Karplus, M. (2009) CHARMM: the biomolecular simulation program. *J. Comput. Chem. 30*, 1545−1614.

(20) Phillips, J. C., Braun, R., Wang, W., Gumbart, J., Tajkhorshid, E., Villa, E., Chipot, C., Skeel, R. D., Kalé, L., and Schulten, K. (2005) Scalable molecular dynamics with NAMD. *J. Comput. Chem. 26*, 1781−1802.

(21) MacKerell, A. D., Jr., Bashford, D., Bellott, M., Dunbrack, R. L., Jr., Evanseck, J. D., Field, M. J., Fischer, S., Gao, J., Guo, H., and Ha, S. (1998) All-atom empirical potential for molecular modeling and dynamics studies of proteins. *J. Phys. Chem. B 102*, 3586−3616.

(22) Essmann, U., Perera, L., Berkowitz, M. L., Darden, T., Lee, H., and Pedersen, L. G. (1995) A smooth particle mesh Ewald method. *J. Chem. Phys. 103*, 8577−8593.

(23) Gao, J., Xia, X., and George, T. F. (1993) Importance of bimolecular interactions in developing empirical potential functions for liquid ammonia. *J. Phys. Chem. 97*, 9241−9247.

(24) Ben-Naim, A., and Marcus, Y. (1984) Solvation thermodynamics of nonionic solutes. *J. Chem. Phys. 81*, 2016.

(25) Zwanzig, R. W. (1954) High-temperature equation of state by a perturbation method. I. Nonpolar gases. *J. Chem. Phys. 22*, 1420−1426.

(26) Orabi, E. A., and Lamoureux, G. (2012) Cation-π and π-π interactions in aqueous solution studied using polarizable potential models. *J. Chem. Theory Comput. 8*, 182−193.

(27) Liu, P., Dehez, F., Cai, W., and Chipot, C. J. (2012) A toolkit for the analysis of free-energy perturbation calculations. *J. Chem. Theory Comput. 8*, 2606−2616.

(28) Humphrey, W., Dalke, A., and Schulten, K. (1996) VMD: visual molecular dynamics. *J. Mol. Graphics 14*, 33−38.

(29) Luzhkov, V. B., Almlöf, M., Nervall, M., and Aqvist, J. (2006) Computational study of the binding affinity and selectivity of the bacterial ammonium transporter AmtB. *Biochemistry 45*, 10807−10814.

(30) Lin, Y., Cao, Z., and Mo, Y. (2006) Molecular dynamics simulations on the Escherichia coli ammonia channel protein AmtB: mechanism of ammonia/ammonium transport. *J. Am. Chem. Soc. 128*, 10876−10884.

(31) Ullmann, R. T., Andrade, S. L., and Ullmann, G. M. (2012) Thermodynamics of transport through the ammonium transporter Amt-1 investigated with free energy calculations. *J. Phys. Chem. B 116*, 9690−9703.

(32) Javelle, A., Severi, E., Thornton, J., and Merrick, M. (2004) Ammonium sensing in Escherichia coli. Role of the ammonium transporter AmtB and AmtB-GlnK complex formation. *J. Biol. Chem. 279*, 8530−8538.

(33) Bruce, L. J., Guizouarn, H., Burton, N. M., Gabillat, N., Poole, J., Flatt, J. F., Brady, R. L., Borgese, F., Delaunay, J., and Stewart, G. W. (2009) The monovalent cation leak in overhydrated stomatocytic red blood cells results from amino acid substitutions in the Rh-associated glycoprotein. *Blood 113*, 1350−1357.

(34) Genetet, S., Ripoche, P., Picot, J., Bigot, S., Delaunay, J., Armari-Alla, C., Colin, Y., and Mouro-Chanteloup, I. (2012) Human RhAG ammonia channel is impaired by the Phe65Ser mutation in overhydrated stomatocytic red cells. *Am. J. Physiol.: Cell Physiol. 302*, C419−C428.

(35) Hub, J. S., Winkler, F. K., Merrick, M., and de Groot, B. L. (2010) Potentials of mean force and permeabilities for carbon dioxide, ammonia, and water flux across a Rhesus protein channel and lipid membranes. *J. Am. Chem. Soc. 132*, 13251−13263.